Journal of Molecular Structure 1143 (2017) 344–354

Contents lists available at ScienceDirect

Journal of Molecular Structure

journal homepage: http://www.elsevier.com/locate/molstruc

Blue emitting 1,8-naphthalimides with electron transport properties for organic light emitting diode applications

Hidayath Ulla [a, *], M. Raveendra Kiran [a], B. Garudachari [b], T.N. Ahipa [c], Kartick Tarafder [a], Airody Vasudeva Adhikari [b], G. Umesh [a], M.N. Satyanarayan [a]

[a] Department of Physics, National Institute of Technology Karnataka, Mangalore, 575025, India
[b] Department of Chemistry, National Institute of Technology Karnataka, Mangalore, 575025, India
[c] Centre for Nano and Material Sciences, Jain University, Bangalore, 562 112, India

ARTICLE INFO

Article history:
Received 1 March 2017
Received in revised form
18 April 2017
Accepted 20 April 2017
Available online 29 April 2017

Keywords:
Blue
OLEDs
Electron-transport
Naphthalimide
Solvatochromism
DFT/TD-DFT

ABSTRACT

In this article, the synthesis, characterization and use of two novel naphthalimides as electron-transporting emitter materials for organic light emitting diode (OLED) applications are reported. The molecules were obtained by substituting electron donating chloro-phenoxy group at the C-4 position. A detailed optical, thermal, electrochemical and related properties were systematically studied. Furthermore, theoretical calculations (DFT) were performed to get a better understanding of the electronic structures. The synthesized molecules were used as electron transporters and emitters in OLEDs with three different device configurations. The devices with the molecules showed blue emission with efficiencies of 1.89 cdA^{-1}, 0.98 lmW^{-1}, 0.71% at 100 cdm^{-2}. The phosphorescent devices with naphthalimides as electron transport materials displayed better performance in comparison to the device without any electron transporting material and were analogous with the device using standard electron transporting material, Alq_3. The results demonstrate that the naphthalimides could play a significant part in the progress of OLEDs.

1. Introduction

Organic π-conjugated materials have attracted considerable research interest because of their use in modern day organic light-emitting diode (OLED) applications [1–4]. One of the key challenges in developing efficient OLEDs is to balance charge injection and transport from both cathode and anode to the emissive layer in the device structure [5–7]. In most of the current organic luminescent materials, electron mobility is usually few orders of magnitude smaller than hole mobility. Hence, by introducing an electron-transport layer (ETL) in the device architecture, the efficiency of OLEDs can be considerably enhanced [3,8]. The potential ETL materials are supposed to have adequately high electron affinity (>3.0 eV) in order to facilitate electron injection from the commonly used metal cathode (Al). Alq_3 has been widely studied as ETL material for OLEDs [7]. Recently, heterocyclic molecules have emerged as promising class of electron-transport materials for OLEDs [3,8–10]. 1,8-naphthalimides have shown considerable promise and are the most frequently studied candidates [11]. The molecules possess wide energy band-gap and low reduction potentials. The excited-state properties in these molecules can be significantly altered by the nature of the substituent present in the aromatic ring [12,13]. The existence of electron-deficient centre usually make these molecules attain high electron affinity which authenticates the possibility of their use as electron-transporting or hole-blocking materials in OLEDs [11]. One option to accomplish this is by introducing electron-donating groups at the C-4 position of 1,8-naphthalimide [12]. Electron-donating substituents at the C-4 position induce a polar charge-transfer excited state, which usually increase the PL emission [14]. In this article, we have synthesized and characterized two novel naphthalimides [**4** and **5**] by nucleophilic substitutions of electron donating chloro-phenoxy group at the C-4 position of 1,8-naphthalimide. We have investigated the naphthalimides as electron-transport as well as electroluminescent materials for OLED applications. Our results show that the materials are potential candidates for electron-transport and/or blue emitters and could play a significant part in the growth of OLEDs.

* Corresponding author.
E-mail address: ulla.hid@gmail.com (H. Ulla).

http://dx.doi.org/10.1016/j.molstruc.2017.04.103
0022-2860/

2. Experimental

2.1. Materials and methods

All the starting reagents and materials obtained from commercial sources (Sigma Aldrich) were used without further purification. Spectroscopic grade organic solvents were used for spectral analysis. The reactions were performed under the blanket of Nitrogen (N_2). NMR, FT-IR and mass spectra were used to confirm the chemical structures of the molecules. NMR spectra were acquired on a Bruker Ascend 400 MHz NMR Spectrometer at a working frequency of 400 MHz at room temperature in DMSO-d_6 as solvent using tetramethylsilane (TMS) as internal standard. The chemical shifts are given as δ in ppm. The mass spectra were recorded using API 2000 LC/MS/MS system and LC-MS-Agilent 1100 series. FT-IR spectra were obtained using a Thermo Nicolet AVATAR 330-FT-IR spectrophotometer. Thin layer chromatography on silica gel coated aluminium sheets (silica gel 60 F254) were used to access and monitor the progress and completion of the reactions. The optical properties of the molecules in solution and thin solid film form were investigated using UV–visible (UV–vis) spectrophotometer (Ocean Optics Inc. SD 2000) and Fluoromax-4 TCSPC spectrophotometer (Horiba Jobin Yvon) at room temperature. A 150 W xenon lamp was used as the excitation source. The spectral data were obtained using FluorEscence software and OrginPro software was used for data analysis. The PL lifetime measurements were done using the same spectrophotometer attached with a NanoLED (350 nm) pulsed excitation source using the time-correlated single-photon counting (TCSPC) technique at room temperature. The decay data was analysed using Data Analysis Software 6 (DAS6). Based on the absorption and PL spectra of the molecules in chloroform ($CHCl_3$), the PL quantum yield (Φ_{PL}) of the molecules were calculated by a comparative method using 9,10-diphenylanthracene ($\Phi_{ref} = 0.90$ in cyclohexane) as standard [15]. Thermogravimetric analysis (TGA) was recorded using EXSTAR 6000, TG/DTA 6300 thermal analyzer. The melting points of the molecules were obtained from differential scanning calorimetry (DSC) using a SHIMADZU DSC-60. DSC and TGA measurements were performed under nitrogen atmosphere. The surface morphology of organic films prepared by thermal evaporation was characterized by Park System XE-70 atomic force microscope (AFM) under ambient conditions in non-contact mode. The electrochemical studies of the molecules in acetonitrile (10^{-3} M) were studied using AUTOLAB PGSTAT-30 electrochemical analyzer at a constant scan rate: 10 mV s^{-1} at room temperature by cyclic voltammetry (CV) measurements in a conventional three-electrode cell system. CV of the molecules in acetonitrile (10^{-3} M) were performed with tetrabutyl ammonium hexafluoro phosphate solution (0.1 M in acetonitrile) as supporting electrolyte and $Ag/AgNO_3$ (in 0.1 M acetonitrile) as reference electrode; platinum plays a dual role as working electrode and counter electrode [12]. The measurements were done in N_2 atmosphere and before each experiment, all the solutions in the cell were purged with ultrahigh-pure N_2 for 10–15 min. Ferrocene/ferrocenium (Fc/Fc^+) redox system was used as internal standard to calibrate each measurements [12].

2.2. Materials synthesis

2.2.1. 6-(4-chlorophenoxy)-2-(2-hydroxyethyl)-1H-benzo[de] isoquinoline-1,3(2H)-dione (**4**)

4-Chlorophenol (0.28 g, 0.0016 mol) and potassium carbonate (anhydrous, 0.22 g, 0.0016 mol) were mixed into a solution of intermediate **3** (0.5 g, 0.0015 mol) in anhydrous DMF (10 ml). In nitrogen atmosphere, the mixture was stirred for 2 h at 100 °C. The obtained reactant mixture was cooled to reach room temperature. It was then poured into 50 ml of cool water. The subsequent yellow precipitate was amassed and treated with charcoal (ethyl acetate 50 ml) at 40 °C for 1 h. This was the purified using column chromatography (eluent: petroleum ether: ethyl acetate 8:2) to obtain a pale yellow solid. Yield 83%. mp 190–192 °C. IR (KBr ν_{max} cm^{-1}): 777, 848 (C-Cl str); 1038, 1172, 1251, 1360 (–O– str); 1485, 1591, 1651, 1703 (C=O str); 2957 (C-H str); 3297 (O-H str). ^{1}H NMR (400 MHz, DMSO-d_6) δ (ppm): 8.67 (d, $J = 8.0$ Hz, 1H, Ar–H), 8.57 (d, $J = 6.0$ Hz, 1H, Ar–H), 8.42 (d, $J = 8.0$ Hz, 1H, Ar–H), 7.92 (t, $J = 7.2$ Hz, 1H, Ar–H), 7.60 (d, $J = 7.6$ Hz, 2H, Ar–H), 7.35 (d, $J = 7.6$ Hz, 2H, Ar–H), 7.06 (d, $J = 8.0$ Hz, 1H, Ar–H), 4.83 (s, 1H, –OH), 4.15 (s, 2H, $-NCH_2-$), 3.62 (d, $J = 5.6$ Hz, 2H, $-NCH_2-CH_2-$). ^{13}C NMR: 164.06, 163.41, 158.92, 154.08, 133.05, 131.96, 130.95, 129.97, 129.51, 128.57, 127.72, 123.79, 122.86, 117.27. 112.05, 58.28, 42.25, 128.85, 127.78, 122.96, 111.98, 61.46, 21.06. *m/z*: 367 (*M*+1). Yield: 83%.

2.2.2. 2-[6-(4-chlorophenoxy)-1,3-dioxo-1H-benzo[de]isoquinolin-2(3H)-yl]ethyl acetate (**5**)

The solution of **4** (0.2 g, 0.0006 mol) in acetic anhydride (2.5 ml) and acetic acid (2.5 ml) was stirred for 2 h at 130 °C in a round bottom flask. The mixture was cooled to obtain a pale yellow precipitate, which was filtered and purified using column chromatography [12]. Yield 90%. mp. 196–198. IR (KBr ν_{max} cm^{-1}): 780, 860 (C-Cl str); 1023, 1057, 1232, 1361 (–O– str); 1462, 1489, 1576, 1655, 1693, 1745 (C=O str); 2969, 3098 (C-H str). ^{1}H NMR (400 MHz, DMSO-d_6) δ (ppm): 8.70 (d, $J = 8.4$ Hz, 1H, Ar–H), 8.61 (s, 1H, Ar–H), 8.45 (d, $J = 8.0$ Hz, 1H, Ar–H), 7.94 (t, $J = 7.2$ Hz, 1H, Ar–H), 7.61 (d, $J = 6.8$ Hz, 2H, Ar–H), 7.37 (d, $J = 6.8$ Hz, 2H, Ar–H), 7.07 (d, $J = 6.8$ Hz, 1H, Ar–H), 4.32 (s, 4H, $-N(CH_2)_2$-), 1.93 (s, 3H, $-CH_3$). ^{13}C NMR: 170.82, 130.97, 128.85, 127.78, 122.96, 111.98, 61.46, 21.06. *m/z*: 410 (*M*+1). Yield: 90%.

2.3. OLED fabrication and testing

The electroluminescent and electron transport properties of the synthesized naphthalimides were studied by fabricating unoptimized OLEDs using thermal evaporation at a base pressure of 5×10^{-6} Torr. Pre-patterned indium tin oxide (ITO, Kintec, Hong Kong) coated glass substrates, with a sheet resistance of 15 Ω/□ and thickness of 120 nm, were used as anode. Prior to the deposition of organic materials, ITO substrates were cleaned and UV-Ozone treated according to the procedure reported earlier [11]. All the organic and cathode layers were deposited on the ITO substrates sequentially without breaking the vacuum and the devices were never exposed to air during fabrication. F_4TCNQ (2,3,5,6-Tetrafluoro-7,7,8,8-tetracyanoquinodimethane, Sigma Aldrich) was used as hole-injection material (HIL), α-NPD (4,4'-bis[*N*-(1-naphthyl)–*N*-phenyl-l-amino]-biphenyl, Sigma Aldrich) was hole-transport material (HTL), BCP (bathocuproine, Sigma Aldrich) was hole-blocking material (HBL), Alq_3 (tris-(8-hydroxyquinoline) aluminium, Sigma Aldrich) was ETL, $Ir(ppy)_3$ (tris[2-phenylpyridinato-C2,N]iridium(III), Sigma Aldrich) doped CBP (4,4'-bis(9-carbazolyl)-biphenyl, Sigma Aldrich) was phosphorescent emitter, LiF (lithium fluoride, Sigma Aldrich) was electron-injection material (EIL), and Al (aluminium, Alfa Aesar) was cathode. The organic materials were used as received without any further purification. All the organic materials were deposited at a rate of 0.5 Å s^{-1}, whereas LiF and Al were deposited at 0.1 Å s^{-1} and 6 Å s^{-1}, respectively. The thickness and the deposition rates were controlled in situ by a quartz crystal thickness oscillator placed near the substrate. As a final step of the fabrication, cathode was deposited through a shadow mask. The light-emitting area was 1.6 mm^2 as defined by the overlap of the cathode and anode. All the electro-optical properties of the fabricated OLEDs such as current density-voltage-luminance (J-V-L) characteristics and

electroluminescence (EL) were investigated using a computer-controlled, programmable source-meter (Keithley 2400), calibrated Si photodiode (SM1PD2A) and spectrophotometer (Horiba Jobin Yvon iHR320). CIE coordinates were calculated from the EL spectra. Devices were driven under dc conditions. All the device characteristics were performed under ambient and dark conditions without any encapsulation at room temperature.

2.4. Computational methods

Density Functional Theory (DFT) calculations were carried out in order to have a deeper understanding of the electronic states of the naphthalimides using GAUSSIAN 09 package. A Becke–Lee–Yang–Parr hybrid exchange-correlation (closed shell) three-parameter functional (B3LYP) [16–18] along with 6–311++G (d) basis set were used in the simulation to obtain the geometry optimization of the isolated molecules. In each case, the molecular structure was completely optimized by using Berny's optimization algorithm, which uses redundant internal coordinates. The convergence to the minima on the potential energy surface was confirmed by calculating the harmonic vibrational wavenumbers using analytic second derivatives and properly scaled down to control the systematic errors caused by incompleteness of the basis set. Since time dependent DFT (TD-DFT) is a powerful and efficient tool to study the ground and excited state properties, we have used this method it considering the same B3LYP exchange-correlation function with 6–311++G (d,p) basis set to obtain the UV–Visible absorption spectra.

3. Results and discussion

3.1. Synthesis and molecular geometry

Scheme 1 depicts the detailed synthetic route that was adopted for the synthesis of **4** and **5** using nucleophilic substitution of chloro-phenoxy electron donating group at the C-4 position of naphthalimide moiety. The synthesis of intermediates **1** (5-Bromoacenaphthene), **2** (4-Bromo-1,8-naphthalic Anhydride) and **3** (6-bromo-2-(2-hydroxyethyl)-1H-benzo[de]isoquinoline-1,3(2H)-dione) were done as per the reported procedure with a slight modification [19]. **5** was prepared by the acetylation of **4** [12]. The molecular structures determined by NMR, FT-IR and mass spectra are in accordance with the proposed structures as well as the theoretically obtained optimized structures. Both the molecules readily dissolve in common organic solvents. The molecules have similar structure where the bromo group at the C-4 position of intermediate **3** is replaced by chloro-phenoxy group to obtain **4**. By replacing C_2H_5O attached to the nitrogen atom in **4** by C_4H_7O, **5** is obtained. From the energy-optimized geometry, we have not observed any significant change in the bond length and bond angle at the central part of both the molecules. However, the different ligand attached to the *N*-atom rearranges the energy labels of molecular orbitals. The optimized structures of **4** and **5** are shown in Fig. 1.

3.2. Optical properties

Studying the optical properties is vital in understanding the functioning of organic materials in devices. On irradiation, the optical properties of naphthalimides are normally associated with chromophoric system's polarization and are governed by the nature of the substituents [20]. Absorption of light in these materials lead to an internal charge transfer (CT) excited state which results in the donor–acceptor interactions (D-π-A) between the electron-donating substituents at the C-4 position and the electron-accepting carbonyl groups. These interactions may be prompted by the environmental effect of different media, especially the polarity of organic solvents. The effect of the solvent polarity is

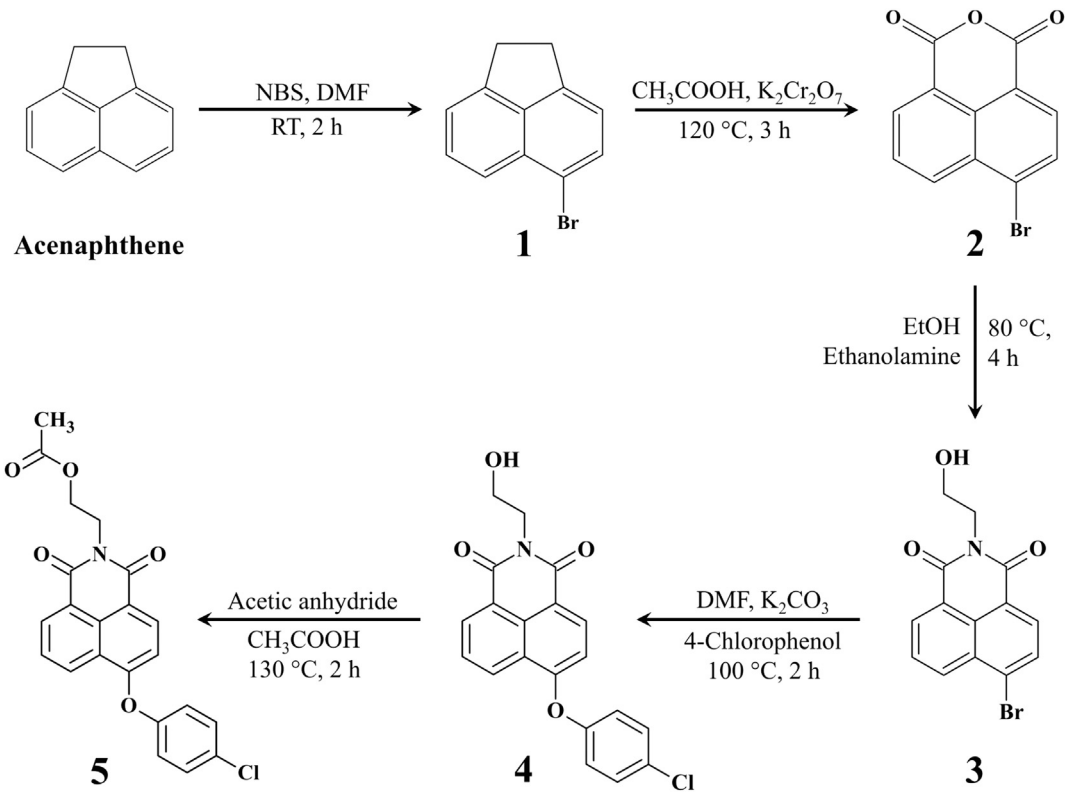

Scheme 1. The synthetic route to naphthalimides.

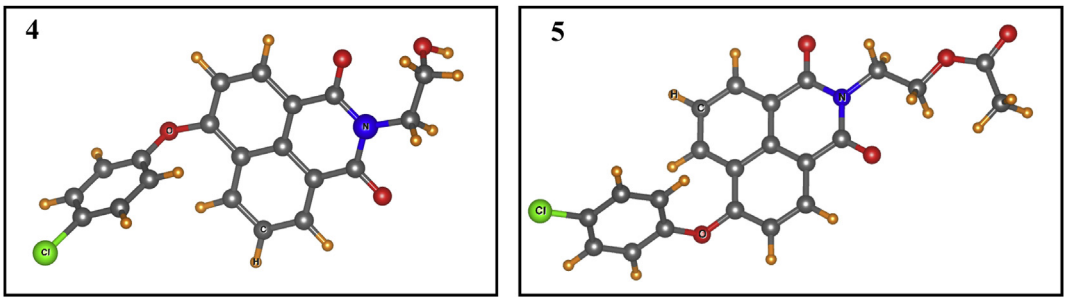

Fig. 1. Molecular structures of naphthalimides **4** and **5** using DFT optimization.

investigated by studying basic optical properties of **4** and **5** in both protic and aprotic organic solvents (10^{-5} M) of different polarities and thin solid film using UV–Vis absorption and PL spectroscopy. The optical data is tabulated in Table 1 and Table SI1.

At room temperature, intermediate **3** which has a bromo group (electron-withdrawing) at C-4 position, shows wavelength absorption maximum (λ_{abs}) of 340 nm (shoulder peak at 354 nm) in $CHCl_3$ [12]. By substituting chloro-phenoxy group which is electron-donating at the C-4 position (**4** and **5**) of intermediate **3** results in the bathochromic shift of ~20 nm in λ_{abs}, thus exhibiting that the lowest singlet excited state has CT nature. Both the molecules show quite similar broadband UV–Vis absorption characteristics (Fig. 2a) with λ_{abs} of 363 nm (**4**) and 362 nm (**5**). This shift may be ascribed to the π-π* electronic transitions occurring between the chloro-phenoxy substituent (electron-donating) at the C-4 position to the carbonyl groups (electron-accepting) in the naphthalimide moiety. The absorption of the molecules is evidently concentrated on the naphthalimide moiety. The lowest excited state is prevalent in π-π* character for 1,8-naphthalimides. A small bathochromic shift (~10 nm) can be seen in λ_{abs} of the thin film (Fig. 2) compared to that in $CHCl_3$, with λ_{abs} shifting to 374 nm (**4**) and 371 nm (**5**). The shift signifies that the π-π* interactions are weak between the molecules in the thin solid film state, which may arise due to the intermolecular aggregation in condensed state. Using the thin film absorption spectra, the optical energy band gaps (E_g^{opt}) of the molecules calculated using Tauc plots (Fig. 2b) considering direct allowed transitions ($(\alpha h\nu)^2$ versus $h\nu$) are 3.04 eV and 2.99 eV, respectively for **4** and **5**. The molar extinction coefficients (log ε) are high (4.3 l mol^{-1} cm^{-1}) which indicates that the long wavelength absorption band has CT nature which may be due to the $S_0 \rightarrow S_1$ transitions.

Time-dependent DFT (TD-DFT) calculations in vacuum were performed on electronic absorption spectrum in order to have a better perceptive of the absorption spectra. Only the lowest six singlet-to-singlet spin-allowed excited states for both the molecules were considered. The generated spectra of **4** and **5** together with experimental observation are presented in Fig. 2a. The calculated excitation energies together with oscillator strength (f) and λ_{abs} are shown in Table 1. In general, UV spectrum of naphthalimides are investigated by the band assigned to the π to π* transition which is also observed in our calculation. In addition, high intensity absorption peak at 350 nm and 348 nm for **4** and **5**, respectively can be observed. Fig. 2a shows reasonably good agreement between the theory and experimental absorption spectra. A slight deviation in the peak position is expected due to the solvent used in experiment. The molecules exhibited intense blue PL emission corresponding to $S_1 \rightarrow S_0$ transition in $CHCl_3$ and in thin solid film, which may be ascribed to the CT interactions between the substituent donor group and carbonyl group acceptors in the moiety.

Intermediate **3** exhibits weak PL with maximum (λ_{PL}) at 406 nm in $CHCl_3$ due to the presence of bromo-substituent at the C-4 position which is electron-withdrawing in nature [12]. On substituting the bromo group in intermediate **3** with the chloro-phenoxy group (**4** and **5**), the λ_{PL} was bathochromic shifted (~20 nm) to 426 nm (**4**) and 422 nm (**5**) with full width half maximum (FWHM) of ~45 nm as shown in Fig. 2a. The observed shifts (Table 1) can be attributed to the introduction of the substituent which lead to the formation of D-π-A structures. Similar to UV–Vis absorption, the λ_{PL} of **5** is hypsochromic shifted (4 nm) compared to that of **4**. Studying the thin film PL of the molecules is important from the viewpoint of device applications. The PL spectra in thin solid films have similar shape to those observed in $CHCl_3$, with λ_{PL} bathochromically shifted to 462 nm (**4**) and 458 nm (**5**) with FWHM of ~60 nm. The energy of activation of the first excited state (E_{S1}) in $CHCl_3$obtained from the point of intersection of absorption and PL spectra, has the values of 312 (**4**) and 316 (**5**) kJ mol^{-1}. The Stokes' shifts (υ_{st}) of the molecules (Table 1) have high values of

Table 1
Photo-physical data of the synthesized naphthalimides.

Cpd.	λ_{abs} (nm)[a,b]	λ_{abs} (nm)[c]	λ_{Em} (nm)[a,b]	Φ_{PL}[d]	FWHM (nm)[a,b]	log ε[e]	E_{S1}[f]	υ_{st} (cm^{-1})[a,b]	f[g]	E_{PL}[h]	E_g^{opt} (eV)[i]	CIE coordinates[a,b]	
												x	y
4	363 (374)	350	426 (462)	0.28	44 (59)	4.339	312	4074 (5093)	0.307 (0.279)	0.33	3.04	0.155 (0.144)	0.050 (0.143)
5	362 (371)	348	422 (458)	0.26	46 (58)	4.268	316	3928 (5120)	0.298 (0.298)	0.21	2.99	0.155 (0.145)	0.044 (0.129)

[a] Recorded in 10^{-5} M $CHCl_3$ Solution.
[b] Values in parantheses are recorded in thin solid film state.
[c] Calculated using DFT.
[d] Relative PL quantum yield (Φ_{PL}) of naphthalimide solution in 10^{-5} M $CHCl_3$ using 9,10-diphenylanthracene in cyclohexane ($\Phi_{ref} = 0.90$) as standard.
[e] Molar extinction coefficients (l mol^{-1} cm^{-1}).
[f] Energy state of activation of the first excited state (kJ mol^{-1}).
[g] Oscillator strength in $CHCl_3$, DFT calculated value (in parentheses).
[h] Energy yields of PL.
[i] Optical band gap by Tauc plots of solid state absorption spectra.

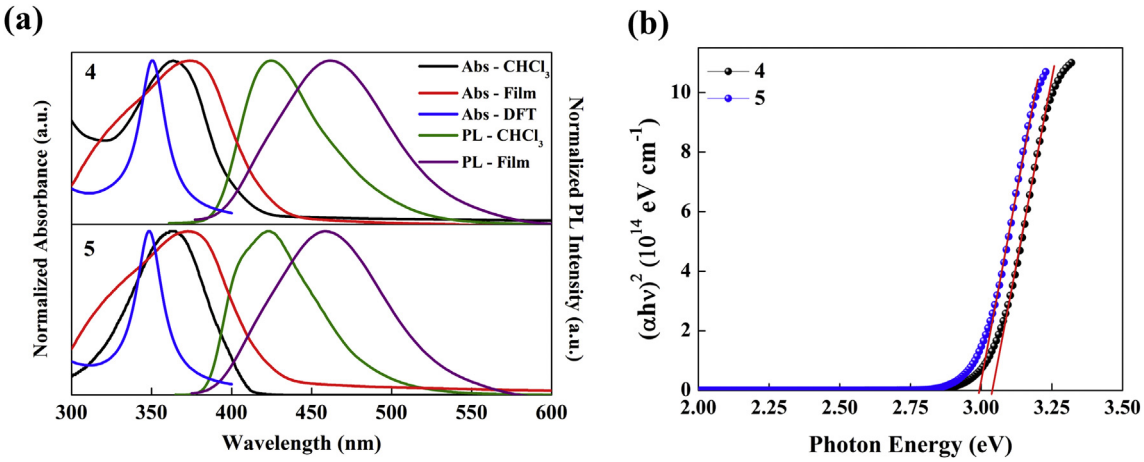

Fig. 2. (a) UV–Vis absorption and PL spectra of the naphthalimides **4** and **5** obtained in $CHCl_3$ solution, thin solid film form and TD-DFT calculations; (b) Optical band-gap determination using Tauc plots.

~4000 cm^{-1} ($CHCl_3$) and ~5100 cm^{-1} (thin films), confirming that the absence of reabsorption of the emitted radiation. The oscillator strengths of the molecules are 0.307 (**4**) and 0.298 (**5**). Both the υ_{st} and *f* values of the molecules are comparable with reported 1,8-naphthalimides [11–13,15]. PL quantum yield (Φ_{PL}) of the molecules are 0.28 (**4**) and 0.26 (**5**). The calculated energy yields of PL (E_{PL}) are 0.33 (**4**) and 0.21 (**5**), which can also be used instead of Φ_{PL}. The values of Φ_{PL} and E_{PL} are higher than their analogous derivatives [11,15]. The performance of the materials in the EL devices can be estimated by relating the emission color by means of *CIE* chromaticity coordinates. These CIE coordinates (Table 1) calculated using the PL spectra excited at 330 nm (in $CHCl_3$) and 360 nm (thin films) are located in the deep blue region of the chromaticity diagram (Fig. SI1).

The absorption spectral data of the molecules in solvents of varying polarity are summarized in Table SI1. A small effect on the λ_{abs} of the molecules was observed with change in solvent nature suggests that in the ground state, solvent effect is very weak as reported in the case of other 1,8-naphthalimides [13]. The absorption spectra of the molecules (Figs. SI2 and SI3) in cyclohexane and hexane are well structured. A loss in the vibrational fine structure occurs by the use of polar solvents. A bathochromic shift in λ_{abs} was noticed for molecules from hexane (~338 nm) to water (~361 nm), signifying a red shift in λ_{abs} for polar solvents. On the other hand, λ_{abs} peak position remains immune to the varying polarity of the polar protic and polar aprotic solvents indicating that solvent polarity has slight impact on the absorption spectra of the molecules. The absence of specific effects in protic solvents shows absence of intermolecular H-bond formation in the molecules' ground state [21]. The PL emission spectra (Figs. SI2 and SI3) demonstrate solvent dependent shifts in emission maxima. Similar to the absorption characteristics, both the molecules showed structured emission in non-polar solvents; however, in the case of mild and high polarity solvents, the molecules exhibited broadband structure-less emission without any clear vibrational structure. As can be seen in Figs. SI2 and SI3, an increase in solvent polarity, i.e., from non-polar to polar solvents, resulted in bathochromic shifts. For instance, an enormous bathochromic shift 77 nm was observed in the case of **4** when changing the medium from hexane to water, which was not noticed in the absorption spectra. This shift indicates that the stabilisation of the solvent is more prominent in the excited states when compared to the ground states. As can be seen from Table SI1, there was a significant increase in the Stokes' shift of **4** from 3570 cm^{-1} in hexane and increases to 6997 cm^{-1} in water. Similar kind of behaviour was also observed for **5** and other 1,8-naphthalimides.

The variations of the dipole moments in ground and excited states can be analysed to observe the response of the molecules to solvent polarity, which can be estimated from Lippert–Mataga (LM) equation [22].

$$\Delta\nu_{st} = (\bar{\nu}_{abs} - \bar{\nu}_{PL}) = \frac{2\Delta f}{hca^3}\Delta\mu^2 \quad (1)$$

where $\bar{\nu}_{abs}$ and $\bar{\nu}_{PL}$ are respectively, the wave numbers of the absorbance and PL emission in cm^{-1}, *h* is the Planck's constant, *c* is the speed of light, *a* is the Onsagar radius of the cavity in which the fluorophore resides [23], $\Delta\mu$ *is* change in the dipole moment and Δf is the orientation polarizability involving the dielectric constant (ε) and refraction index (*n*) of the solvents as given by equation (2). Fig. SI4 represents the LM plot of the molecules in different solvents.

$$\Delta f = \frac{\varepsilon - 1}{2\varepsilon + 1} - \frac{n^2 - 1}{2n^2 + 1} \quad (2)$$

The gross solvent polarity indicator scale such as empirical parameter of solvent polarity E_T30 becomes more applicable while considering the case of charge transfer in a molecule [24]. Fig. SI5 shows the variation of Stokes' shift with the E_T30 values of the solvents revealing a related tendency for protic and aprotic solvents. Fig. SI5 clearly shows the significant influence of the solvent polarity on the spectral properties of the molecules.

The emission mechanism is studied by investigating PL decay lifetime as it decides the suitable use of the materials in devices. The efficiency of the radiative recombination is directly proportional to the particular transition decay time. Time resolved PL spectroscopy was used to study PL decay spectrum of the molecules in $CHCl_3$ at 426 nm (**4**) and 422 nm (**5**) for blue emission by TCSPC technique with a 350 nm pulsed NanoLED as source of excitation at room temperature. The obtained results are tabulated in Table SI2 and the decay profiles of the molecules are plotted in Fig. 3. The lifetime data obtained for the molecules were fitted to a double exponential function using DAS6 software as presented in equation (3), where τ_1 and τ_2 are the decay lifetimes of the luminescence with amplitudes A_1 and A_2, respectively. The observed lifetimes are τ_1 ~ 0.54 ns and τ_2 ~ 2.38 ns for **4**; and τ_1 ~ 0.91 ns and τ_2 ~ 3.63 ns for **5**. For double-exponential decay, the average lifetime, τ_{av}, is typically tailored to replace the various parameters of the

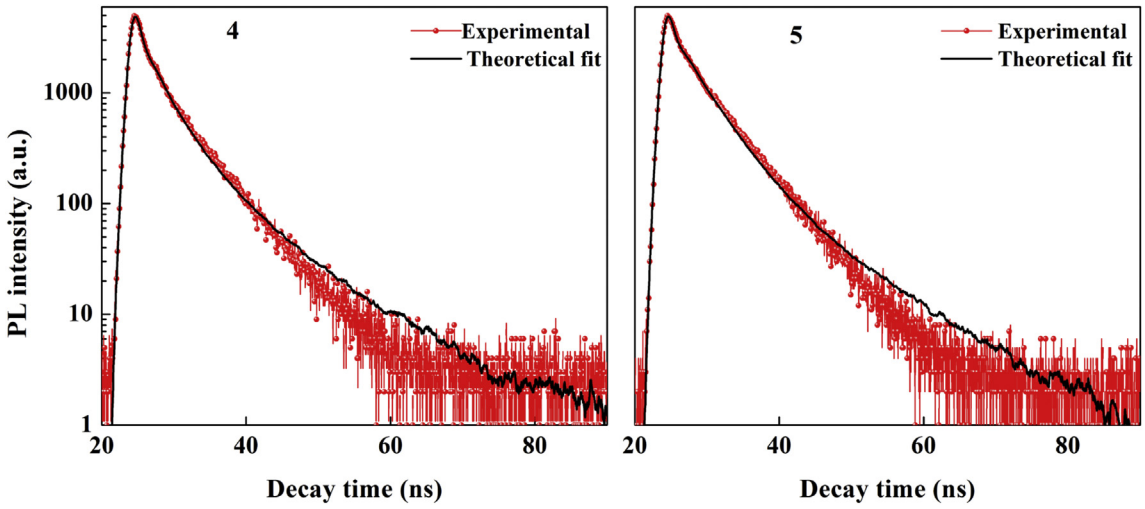

Fig. 3. Time resolved PL spectra of naphthalimides **4** and **5.**

luminescence lifetime, which is established by equation (4) [25]. The calculated average lifetime are 1.91 ns (**4**) and 3.19 ns (**5**). It can also be noted from the decay profile that the triplet energy transfer is totally suppressed in both the molecules. These results are extremely suitable for display applications.

$$F(t) = A_1 \exp\left(-\frac{t}{\tau_1}\right) + A_2 \exp\left(-\frac{t}{\tau_2}\right) \quad (3)$$

$$\tau_{av} = \frac{(A_1\tau_1^2 + A_2\tau_2^2)}{(A_1\tau_1 + A_2\tau_2)} \quad (4)$$

3.3. Electrochemical properties

The electrochemical properties of the naphthalimides were investigated by CV in order to determine HOMO and LUMO energy-levels as well as to explore the charge injection capabilities. The CV measurements were performed in 10^{-3} M acetonitrile on platinum containing 0.1 M Bu_4NPF_6 as supporting electrolyte, $Ag/AgNO_3$ electrode as reference and ferrocene/ferrocenium as calibrant [12] at a scanning rate of 10 V^{-1}. Prior to the measurements, all the solutions were purged with N_2. The electrochemical data of the molecules are summarized in Table 2. The cathodic scans revealed quasi-reversible reduction waves with onset reduction potentials of −1.47 V and −1.41 V versus $Ag/AgNO_3$, respectively for **4** and **5**; whereas the anodic scans exhibited irreversible waves with onset oxidation potentials of 1.44 and 1.47 V vs. $Ag/AgNO_3$, respectively for **4** and **5**. The energy-levels of **4** and **5** were predicted by comparing the onset potentials of ferrocene (4.8 eV versus vacuum). The HOMO energy-levels obtained from the onset of the oxidation wave (HOMO = - 4.8 - E^{ox}_{onset}) are 6.24 eV (**4**) and 6.27 eV (**5**); the LUMO energy-levels estimated using the onset of the reduction wave (LUMO = - 4.8 - E^{red}_{onset}) are 3.33 eV (**4**) and 3.39 eV (**5**). Both the HOMO and LUMO energy-levels of **4** and **5** are lower than their reported counterparts [11,15]. It is interesting to note that the HOMO-LUMO energy band-gaps of 2.91 eV (**4**) and 2.88 eV (**5**) are fairly near to the calculated optical band gaps within experimental error. The surface of the HOMO-LUMO orbitals obtained by DFT calculations are depicted in Fig. 4. The computationally calculated HOMO-LUMO values are in agreement with the electrochemical studies (Table 2). These low-lying LUMO energy-levels lead to high electron affinity, which reveals that the molecules have potential as electron-transporting (n-type) materials for OLED applications.

3.4. Thermal properties and surface morphology

For organic optoelectronic device applications, materials with high thermal stability is desired. In addition, the high thermal stability also enhances the device lifetime. The thermal behaviour, including the decomposition temperatures (T_d) and melting points (T_m) were studied for **4** and **5** using TGA and DSC. The thermal stabilities were investigated by TGA in the temperature range 30–600 °C and melting points were evaluated by performing DSC. A constant heating rate of 10 °C min^{-1} was maintained to melt and decompose the molecules in N_2 atmosphere (flow rate: 30 ml min^{-1}). The results are summarized in Table 2. The TGA thermograms (Fig. 5a) and the values in Table 2 reveal that the

Table 2
Electrochemical data obtained from cyclic voltammetry measurements along with DFT obtained values for comparison and thermal data of synthesized naphthalimides.

Cpd.	E^{ox}_{onset} versus E_{fc} (V)[a]	E^{red}_{onset} versus E_{fc} (V)[a]	CV measurements			DFT calculations			T_d (°C)[d]	T_m (°C)[e]
			HOMO (eV)	LUMO (eV)	E_g^{EC} (eV)[b]	HOMO (eV)	LUMO (eV)	E_g^{Cal} (eV)[c]		
4	1.44	−1.47	−6.24	−3.33	2.91	- 6.31	−2.44	3.88	299	191
5	1.47	−1.41	−6.27	−3.39	2.88	−6.41	−2.52	3.89	295	197

[a] E^{ox}_{onset} and E^{red}_{onset} are measured vs ferrocene/ferrocenium.
[b] $E_g^{ec} = (E^{ox}_{onset} - E^{red}_{onset})$.
[c] DFT calculations.
[d] Decomposition temperatures at 10% weight loss.
[e] Melting point of the derivatives from DSC.

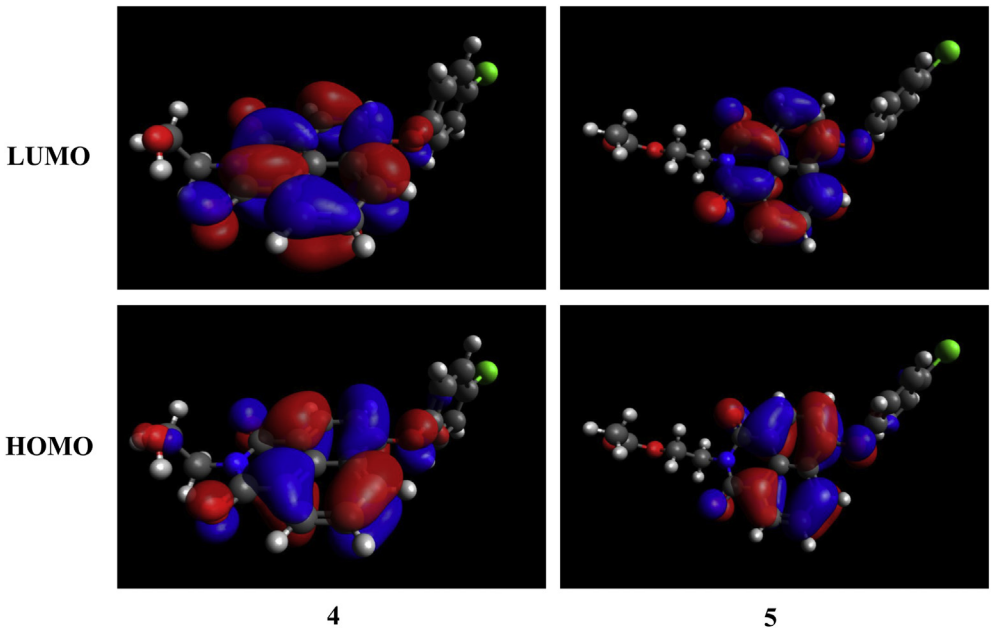

Fig. 4. Pictorial representations of frontier molecular orbital surfaces of the HOMO and LUMO of the naphthalimides 4 and 5 calculated using B3LYP/6−311++G (d,p).

molecules exhibit high T_d. No weight loss was observed at lower temperatures. The molecules show single step in the thermal decomposition process starting at ~235 °C followed with a rapid weight loss of ~60% of the mass occurring in the range 235−330 °C. A steady weight loss was noted on further heating. The molecules possess T_d values of 299 °C (**4**) and 295 °C (**5**) corresponding to 10% weight loss. DSC scans (Fig. 5b) exhibit clear endothermic peaks with T_m of 191 °C (**4**) and 197 °C (**5**). The course of melting points obtained by DSC are well in agreement with the capillary method melting points of the molecules. The capability of the molecules to form amorphous uniform thin films with low roughness value upon vacuum thermal vapour deposition plays a significant role in the functioning of organic electroluminescent devices. The surface morphology of the vacuum-deposited films (50 nm) prepared on n-Si substrates at a deposition rate of 0.5 Å/s has been studied by performing AFM measurements. The three-dimensional AFM images (10 × 10μ) of the molecules are presented in Fig. 6 which shows root-mean-square roughness values of 2.6 nm (**4**) and 3.5 nm (**5**). It can be seen from Fig. 6 as well as the surface roughness values that they are capable of forming quite smooth films. The roughness of deposited films using thermal evaporation technique typically is in the molecular size range. Hence the molecules exhibit good film deposition characteristics and thermal stability.

3.5. Electroluminescent properties

As the final part of the investigation, to study the utility of the synthesized naphthalimides (**Naph**), unoptimized OLEDs were fabricated and characterized. The associated HOMO-LUMO energy-levels of the molecules along with other materials used in the electroluminescent devices are illustrated in Fig. 7. To evaluate the emissive properties of the naphthalimides as emitters, undoped OLEDs were fabricated with the configuration **I**: ITO (120 nm)/α-NPD (30 nm)/**Naph** (35 nm)/BCP (6 nm)/Alq_3 (35 nm)/LiF (1 nm)/Al (150 nm). Here ITO served as a transparent anode. α-NPD was used

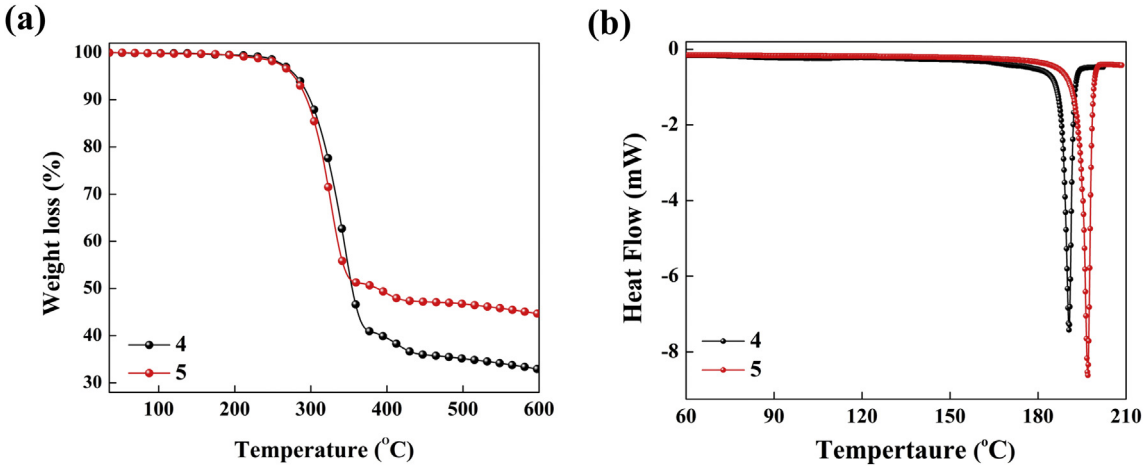

Fig. 5. (a) TGA and (b) DSC thermograms of the naphthalimides under nitrogen.

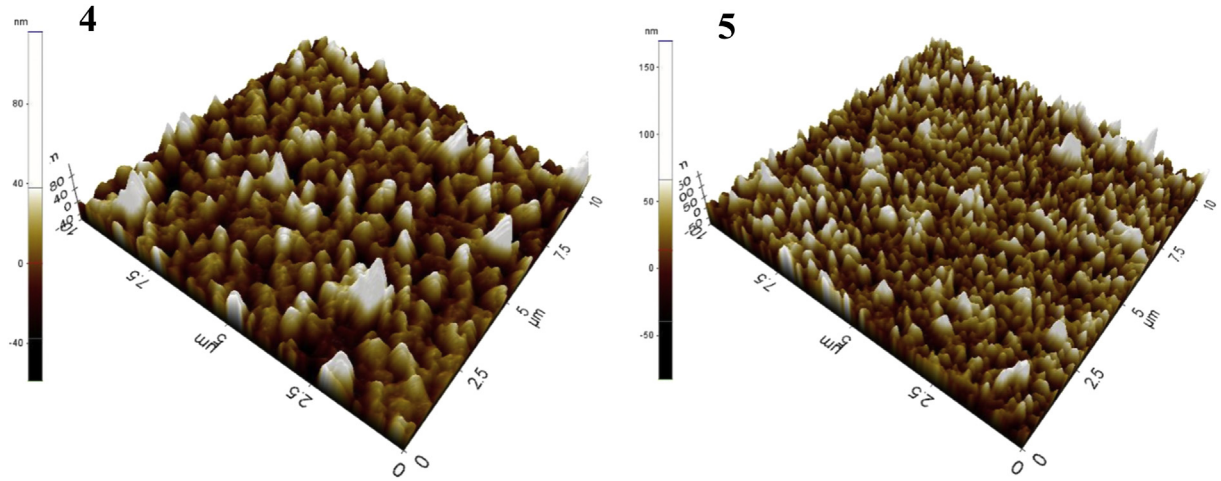

Fig. 6. AFM images of thermally evaporated naphthalimides **4** and **5.**

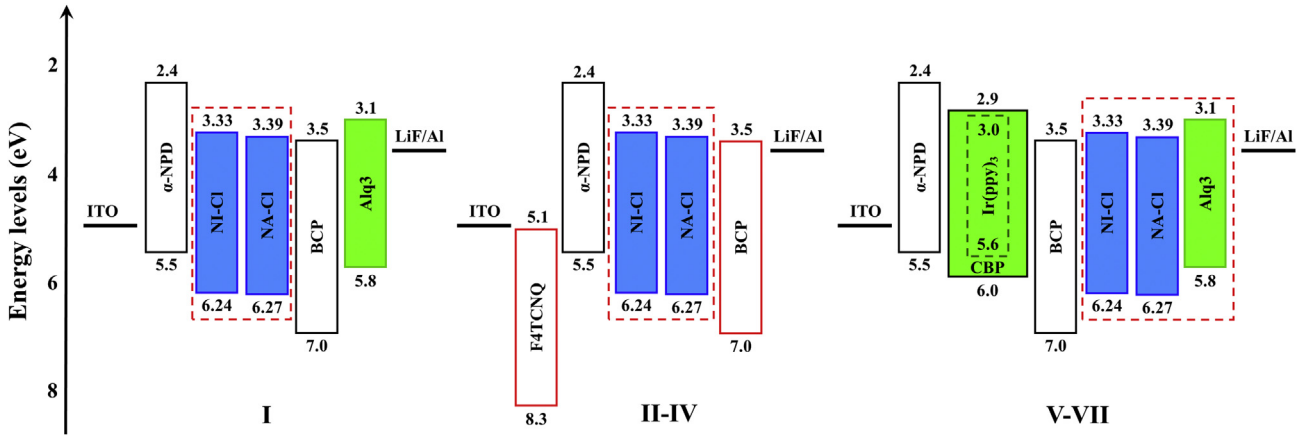

Fig. 7. Energy-level diagram of the materials used in the devices **(I)** Naphthalimides as EL materials; **(II-IV)** Naphthalimides as EL and ETL materials; **(V-VII)** Naphthalimides and Alq_3 as ETL materials.

as the HTL because of it is high HOMO energy. In addition, considering the energy-levels (shown in Fig. 7) of the molecules, α-NPD with a higher LUMO level also plays a role of an effective electron-blocking material. BCP was used as HBL as it assists in confining the reductant holes in the emitting layer which didn't recombine with the electrons in the emitting zone [26]. Alq_3 was used as an ETL. LiF was used as EIL and Al was used as the cathode. The current (η_c), output power (η_p) and external quantum (η_{EQE}) efficiencies of both the devices along with other parameters of the devices are summarized in Table 3. The J-V-L and J-L curves of the fabricated devices are shown in Fig. 8. The relation of current density with varying voltage (Fig. 8a) reveal good diode behaviour. The J-L characteristics (Fig. 8b) show a linear relationship. Both the devices displayed good current density signifying good charge transport capability. The devices utilizing **4** and **5** as emitter materials showed maximum luminance (L_{max}) of 889 and 1072 cdm^{-2} at 15 V; efficiencies of 0.89 and 0.96 cd/A (η_c), 0.21 and 0.23 lm/W (η_p), 0.41 and 0.47% (η_{EQE}), respectively at 100 cdm^{-2}. The turn-on voltage of a device principally depends on the HOMO and LUMO energies of the constituent layers. The HOMO energy-level of α-NPD (−5.5 eV) creates a hole-injection barrier of 0.74 eV at the α-NPD/**4** and 0.77 eV at α-NPD/**5** junctions. Similarly, the electron-injection barriers at the **4**/Alq_3 and **5**/Alq_3 are 0.23 eV and 0.29 eV, respectively as the LUMO energy-level of Alq_3 is 3.1 eV.

Table 3
Electroluminescent performance data of naphthalimides as emissive materials.

Device[a]	V_{onset} (V)[b]	L_{max} (cd m^{-2})[c]	η_c (cd A^{-1})[d]	η_p (lm W^{-1})[d]	η_{EQE} (%)[d]	λ_{em} (FWHM) (nm)[e]	$CIE_{(x,y)}$[f]
4	7.03	889	0.89	0.21	0.41	485 (70)	(0.190, 0.283)
5	6.92	1072	0.96	0.23	0.47	483 (71)	(0.181, 0.279)

[a] Device Configuration **I**: ITO (120 nm)/α-NPD (30 nm)/**Naph** (35 nm)/BCP (6 nm)/Alq_3 (35 nm)/LiF (1 nm)/Al (150 nm).
[b] V_{onset}: turn-on voltage at luminance of 1 cd m^{-2}.
[c] L_{max}: Maximum luminance at 15 V.
[d] Current (η_c), power (η_p) and external quantum efficiencies (η_{ext}) measured at 100 cdm^{-2}.
[e] λ_{em}: Emission wavelength maximum; FWHM: full width half maximum at 15 V.
[f] CIE color coordinates.

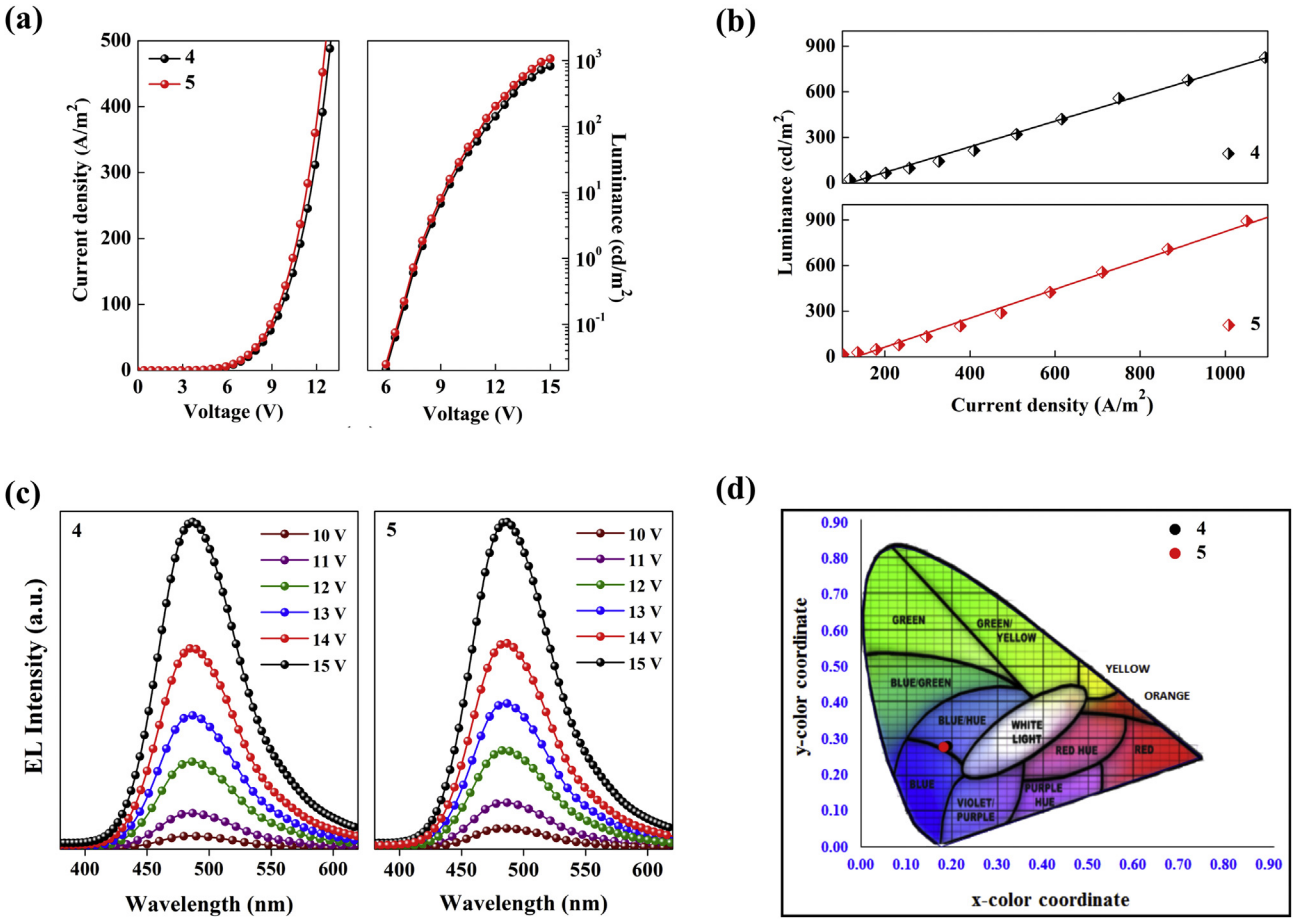

Fig. 8. (a) J-V-L characteristics, (b) J-L characteristics (c) EL spectra at different applied voltages and (d) Chromaticity diagram of the OLEDs with naphthalimides as EL materials.

Hence, the hole-injection barriers might have accounted for slightly high turn-on voltages of 7.03 V (**4**) and 6.92 V (**5**) corresponding to 1 cd m^{-2}. The observed slight variation in the turn-on voltage for **4** and **5** may be due to the difference in the electron-injection band-offsets in the devices. The steady-state EL spectra of the devices with naphthalimides at different applied voltages are depicted in Fig. 8c. The devices showed blue light emission with peaks centred at 485 (**4**) and 483 (**5**) with FWHM of ~70 nm. The narrow FWHM in EL spectra suggest that the molecules are capable of forming good chromaticity devices. The EL spectra closely matches that of the solid film PL spectra of the molecules with a slight bathochromic shifts suggesting emission from the molecules as the major component in EL. The bathochromic shift in EL peaks with respect to PL may be due to interplay of charge carrier versus exciton dynamics and/or due to the result of excimer formation [26]. The CIE chromaticity coordinates were determined using the EL spectra of the devices at 15 V. The chromaticity diagram is shown in Fig. 8d and the CIE coordinates are tabulated in Table 3. Furthermore, as depicted in Fig. 8c, the EL spectra of both the devices showed the same profile without any effect on the shape and EL spectra peak under various driving voltages. Hence, both the devices exhibited excellent spectral stability over a wide range of operating voltages. It is noteworthy that, during the measurements, both the devices did not damage at higher applied electrical voltages, perhaps due to the high thermal stabilities of the molecules. This observation offers the potential use of the molecules in OLED applications.

The role of naphthalimides as both electron transporting and emitting materials was studied by fabricating OLEDs with the configurations **II-IV**: ITO (120 nm)/F_4TCNQ (4 nm)/α-NPD (40 nm)/**Naph** (50 nm)/BCP (6 nm)/LiF (1 nm)/Al (150 nm). Here F_4TCNQ was chosen as a HIL as it efficiently injects holes from the ITO anode to HTL. An optimized thickness of F_4TCNQ was used for better hole injection as reported earlier [27,28]. The device with configuration **II** was fabricated with **4** as an active material without hole injection layer, F_4TCNQ and hole blocking layer, BCP; device **III** with F_4TCNQ and without BCP; and device **IV** with both F_4TCNQ and BCP. The performance data along with other parameters of all the devices are tabulated in Table 4. In assessing the device performance, it is

Table 4
Electroluminescent performance data of OLEDs using naphthalimides as both EL and ETL materials.

Device	V_{onset} (V)[d]	L_{max} (cd m^{-2})[e]	η_c (cd A^{-1})[f]	η_p (lm W^{-1})[f]	η_{EQE} (%)[f]
4[a]	9.67	472	0.45	0.11	0.24
4[b]	6.62	1493	1.79	0.51	0.40
4[c]	6.35	1580	1.87	0.86	0.69
5[c]	6.18	1681	1.89	0.98	0.71

[a] Device Configuration **II**: ITO (120 nm)/α-NPD (40 nm)/**4** (50 nm)/LiF (1 nm)/Al (150 nm).
[b] Device Configuration **III**: ITO (120 nm)/F_4TCNQ (4 nm)/α-NPD (40 nm)/**4** (50 nm)/LiF (1 nm)/Al (150 nm).
[c] Device Configuration **IV**: ITO (120 nm)/F_4TCNQ (4 nm)/α-NPD (40 nm)/**Naph** (50 nm)/BCP (6 nm)/LiF (1 nm)/Al (150 nm).
[d] V_{onset}: turn-on voltage at luminance of 1 cd m^{-2}.
[e] L_{max}: Maximum luminance at 15 V.
[f] Current (η_c), power (η_p) and external quantum efficiencies (η_{ext}) measured at 100 cdm^{-2}.

Table 5
Electroluminescent performance data of OLEDs using of triplet emitter $Ir(ppy)_3$ doped with CBP (with changing ETL).

Device[a]	V_{onset} (V)[b]	L_{max} (cd m^{-2})[c]	η_c (cd A^{-1})[d]	η_p (lm W^{-1})[d]	η_{EQE} (%)[d]
No ETL	12.76	1714	5.39	1.23	0.94
Alq_3	9.09	9650	9.79	2.71	1.70
4	9.23	5341	8.90	1.82	1.39
5	9.14	5962	9.04	1.98	1.46

[a] Device Configuration **II-IV**: ITO (120 nm)/α-NPD (40 nm)/$Ir(ppy)_3$ doped CBP (35 nm)/BCP (6 nm)/**No ETL** or **Alq_3** or **Naph** (30 nm)/LiF (1 nm)/Al (150 nm).
[b] V_{onset}: turn-on voltage at luminance of 1 cd m^{-2}.
[c] L_{max}: Maximum luminance at 21 V.
[d] Current (η_c), power (η_p) and external quantum efficiencies (η_{ext}) measured at 100 cdm^{-2}.

evident from Table 4 that the device **II** without F_4TCNQ and BCP shows low luminance 472 cd m^{-2} and efficiencies of 0.45 cd A^{-1} (η_c), 0.11 lm W^{-1} (η_p) and 0.24% (η_{EQE}). With the inclusion of 4 nm of F_4TCNQ layer (device **III**) there is a considerable increase in luminance (1493 cd m^{-2}) and efficiencies; 1.79 cd A^{-1} (η_c), 0.51 lm W^{-1} (η_p) and 0.40% (η_{EQE}). This can the ascribed to the efficient injection of holes from the anode (ITO) to the hole transport layer (α-NPD) [27,28]. Furthermore, in device **IV**, with the use of BCP as an HBL, there is further increase in the luminance (1580 cd m^{-2}) and efficiencies to 1.87 cd A^{-1} (η_c), 0.86 lm W^{-1} (η_p) and 0.69% (η_{EQE}) 100 cd/m^2. This increase in efficiencies may be due to the confining of redundant holes in the emitting layer. The device structure **IV** used for **5** showed efficiencies of 1.89 cd A^{-1} (η_c), 0.98 lm W^{-1} (η_p) and 0.71% (η_{EQE}) 100 cd/m^2.

The electron transporting nature of naphthalimides were investigated by fabricating phosphorescent OLED with **4** and **5** as ETL materials. Also, OLEDs without any ETL material and with Alq_3 as standard ETL material were fabricated for comparison. Here $Ir(ppy)_3$ doped CBP was used as phosphorescent emitter for all the devices. The device configurations **V-VII** of the fabricated OLEDs are ITO (120 nm)/α-NPD (40 nm)/$Ir(ppy)_3$ doped CBP (35 nm)/BCP (6 nm)/**No ETL** or **Naph** or **Alq_3** (30 nm)/LiF (1 nm)/Al (150 nm). In the device configurations, **V-VII** only ETL was changed, whereas the rest was kept same. In device **V**, no ETL material was used; in device **VI** Alq_3 was used as standard ETL material; whereas, device **VII** was fabricated with **4/5** as ETL materials. The performance data from each of these devices are tabulated in Table 5. The J-V-L characteristics with different ETL materials are shown in Fig. 9a. The J-L characteristics (Fig. 9b) show a linear relationship between current density and luminance. It is evident from Fig. 9 and Table 5 that with the inclusion of **4** as ETL, there is a drastic increase in efficiencies (η_c: 8.9 cd A^{-1}, η_p: 1.82 lm W^{-1}, η_{EQE}: 1.39%) when compared to the device without ETL (η_c: 5.39 cd A^{-1}, η_p: 1.23 lm W^{-1}, η_{EQE}: 0.94%). The device structure **VII** was also used for **5** which showed efficiencies of 9.04 cd A^{-1} (η_c), 1.98 lm W^{-1} (η_p) and 1.46% (η_{EQE}). The EL spectra (Fig. 9c) for all the devices was similar with λ_{max} at 516 nm which is due to $Ir(ppy)_3$ with similar CIE coordinates (0.28, 0.62) (Fig. 9d). The obtained results reveal that by using naphthalimides as ETL, a significant improvement in performance is observed and is comparable to device with Alq_3 as ETL (Table 5). Our investigations reveal that the synthesized molecules

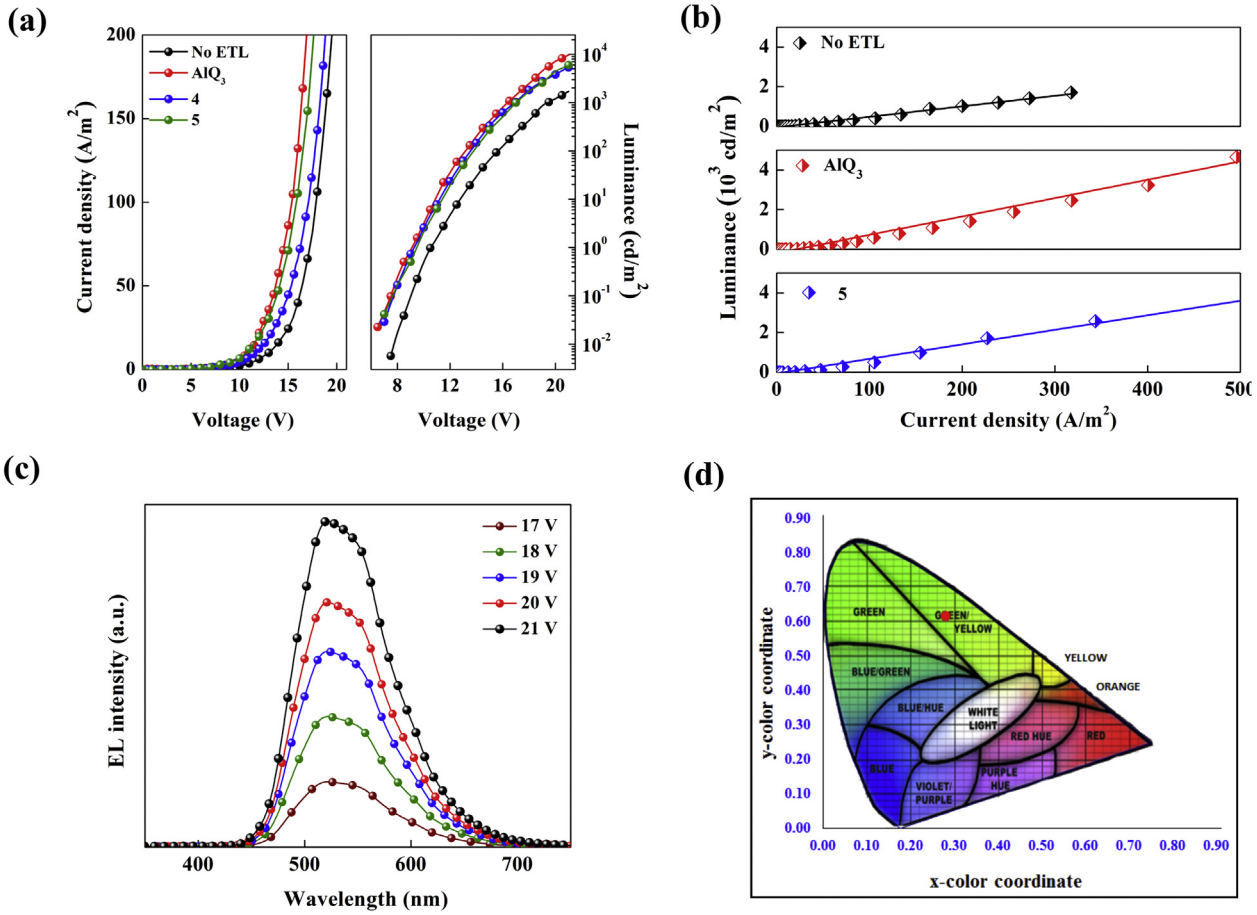

Fig. 9. (a) J-V-L characteristics, (b) J-L characteristics (c) EL spectra at different applied voltages and (d) Chromaticity diagram of the phosphorescent OLEDs without ETL/with Alq_3/Naph as ETL.

show potential as electron transporting emitter materials in OLEDs.

4. Conclusions

Two chloro-phenoxy 1,8-naphthalimides, **4** and **5**, were synthesized and characterized. The molecules show high electron affinity and possess wide band gap which are essential for blue light electroluminescence. The optical properties of the molecules revealed blue PL emission with high Stokes' shifts. The molecules show good thermal stabilities as revealed by thermal properties. The HOMO-LUMO energy-levels of the molecules are low which make them acquire excellent hole-blocking and electron-transporting properties. As emissive materials, OLEDs using naphthalimides showed efficiencies of 0.96 cd/A (V), 0.23 lm/W (η_p) and 0.47% (η_{EQE}). Naphthalimides as both EL and ETL materials showed efficiencies of 1.89 cd/A (η_c), 0.98 lm/W (η_p) and 0.71% (η_{EQE}) revealing that they can act as electron transporting emitters. Furthermore, compared to the phosphorescent OLED without any ETL material (η_c: 5.39 cd/A, η_p: 1.23 lm/W and η_{EQE}: 0.94%), devices with naphthalimides as ETL materials showed good performance (η_c: 9.04 cd/A, η_p: 1.98 lm/W and η_{EQE}: 1.46%); the performance was comparable with standard device with Alq_3 as ETL material. Our results validate that the molecules have potential as undoped blue emitters with electron transport properties and hence can play an important role in the progress of high performance OLED devices.

Acknowledgement

The authors acknowledge Department of Information Technology (Grant No. 12(3)/2010-PDD), India for the financial support. H.U. acknowledge the Department of Physics, NITK, Surathkal, for various facilities and financial support.

Appendix A. Supplementary data

Supplementary data related to this article can be found at http://dx.doi.org/10.1016/j.molstruc.2017.04.103.

References

[1] C.W. Tang, S.A. VanSlyke, Organic electroluminescent diodes, Appl. Phys. Lett. 51 (1987) 913–915, http://dx.doi.org/10.1063/1.98799.
[2] J.H. Burroughes, D.D.C. Bradley, A.R. Brown, R.N. Marks, K. Mackay, R.H. Friend, P.L. Burns, A.B. Holmes, Light-emitting diodes based on conjugated polymers, Nature 347 (1990) 539–541, http://dx.doi.org/10.1038/347539a0.
[3] A.P. Kulkarni, C.J. Tonzola, A. Babel, S.A. Jenekhe, Electron transport materials for organic light-emitting diodes, Chem. Mater. 16 (2004) 4556–4573, http://dx.doi.org/10.1021/cm049473l.
[4] M.L. Tang, Z. Bao, Halogenated materials as organic semiconductors, Chem. Mater. 23 (2011) 446–455, http://dx.doi.org/10.1021/cm102182x.
[5] J.M. Hancock, A.P. Gifford, Y. Zhu, Y. Lou, S.A. Jenekhe, n-Type conjugated oligoquinoline and oligoquinoxaline with triphenylamine endgroups: efficient ambipolar light emitters for device applications, Chem. Mater. 18 (2006) 4924–4932, http://dx.doi.org/10.1021/cm0613760.
[6] C.J. Tonzola, A.P. Kulkarni, A.P. Gifford, W. Kaminsky, S.A. Jenekhe, Blue-light-emitting oligoquinolines: synthesis, properties, and high-efficiency blue-light-emitting diodes, Adv. Funct. Mater. 17 (2007) 863–874, http://dx.doi.org/10.1002/adfm.200600542.
[7] T. Earmme, E. Ahmed, S.A. Jenekhe, Highly efficient phosphorescent light-emitting diodes by using an electron-transport material with high electron affinity, J. Phys. Chem. C 113 (2009) 18448–18450, http://dx.doi.org/10.1021/jp907913d.
[8] G. Hughes, M.R. Bryce, Electron-transporting materials for organic electroluminescent and electrophosphorescent devices, J. Mater. Chem. 15 (2005) 94–107, http://dx.doi.org/10.1039/B413249C.
[9] H. Sasabe, E. Gonmori, T. Chiba, Y.-J. Li, D. Tanaka, S.-J. Su, T. Takeda, Y.-J. Pu, K. Nakayama, J. Kido, Wide-energy-gap electron-transport materials containing 3,5-dipyridylphenyl moieties for an ultra high efficiency blue organic light-emitting device, Chem. Mater. 20 (2008) 5951–5953, http://dx.doi.org/10.1021/cm801727d.
[10] S.-J. Yoo, H.-J. Yun, I. Kang, K. Thangaraju, S.-K. Kwon, Y.-H. Kim, A new electron transporting material for effective hole-blocking and improved charge balance in highly efficient phosphorescent organic light emitting diodes, J. Mater. Chem. C 1 (2013) 2217–2223, http://dx.doi.org/10.1039/C3TC00801K.
[11] H. Ulla, M. Raveendra Kiran, B. Garudachari, M.N. Satyanarayan, G. Umesh, A.M. Isloor, Blue emitting halogen–phenoxy substituted 1,8-naphthalimides for potential organic light emitting diode applications, Opt. Mater. 37 (2014) 311–321, http://dx.doi.org/10.1016/j.optmat.2014.06.016.
[12] Y. Wang, X. Zhang, B. Han, J. Peng, S. Hou, Y. Huang, H. Sun, M. Xie, Z. Lu, The synthesis and photoluminescence characteristics of novel blue light-emitting naphthalimide derivatives, Dyes Pigments 86 (2010) 190–196, http://dx.doi.org/10.1016/j.dyepig.2010.01.003.
[13] N.V. Marinova, N.I. Georgiev, V.B. Bojinov, Facile synthesis, sensor activity and logic behaviour of 4-aryloxy substituted 1, 8-naphthalimide, J. Photochem. Photobiol. Chem. 254 (2013) 54–61.
[14] N.V. Marinova, N.I. Georgiev, V.B. Bojinov, Facile synthesis, sensor activity and logic behaviour of 4-aryloxy substituted 1, 8-naphthalimide, J. Photochem. Photobiol. Chem. 254 (2013) 54–61.
[15] H. Ulla, B. Garudachari, M.N. Satyanarayan, G. Umesh, A.M. Isloor, Blue organic light emitting materials: synthesis and characterization of novel 1,8-naphthalimide derivatives, Opt. Mater. 36 (2014) 704–711, http://dx.doi.org/10.1016/j.optmat.2013.11.017.
[16] A.D. Becke, Density-functional thermochemistry. III. The role of exact exchange, J. Chem. Phys. 98 (1993) 5648–5652, http://dx.doi.org/10.1063/1.464913.
[17] C. Lee, W. Yang, R.G. Parr, Development of the Colle-Salvetti correlation-energy formula into a functional of the electron density, Phys. Rev. B 37 (1988) 785–789, http://dx.doi.org/10.1103/PhysRevB.37.785.
[18] J.P. Perdew, Y. Wang, Accurate and simple analytic representation of the electron-gas correlation energy, Phys. Rev. B 45 (1992) 13244–13249, http://dx.doi.org/10.1103/PhysRevB.45.13244.
[19] P.H. Grayshan, A.M. Kadhim, A.T. Perters, Heterocyclic derivalives of naphthalene-1,8-dicar boxylie anhydride. Part III. Benzo[k,l] thioxanthene-3,4-dicarboximides, J. Heterocycl. Chem. 11 (1974) 33–38, http://dx.doi.org/10.1002/jhet.5570110107.
[20] R.M. Duke, E.B. Veale, F.M. Pfeffer, P.E. Kruger, T. Gunnlaugsson, Colorimetric and fluorescent anion sensors: an overview of recent developments in the use of 1,8-naphthalimide-based chemosensors, Chem. Soc. Rev. 39 (2010) 3936–3953, http://dx.doi.org/10.1039/B910560N.
[21] N.I. Georgiev, V.B. Bojinov, Design, synthesis and photostability of novel 1,8-naphthalimide PAMAM light-harvesting dendrons, J. Fluoresc. 21 (2010) 51–63, http://dx.doi.org/10.1007/s10895-010-0689-y.
[22] R.M. Moustafa, J.A. Degheili, D. Patra, B.R. Kaafarani, Synthesis and detailed photophysical studies of pyrene-based molecules substituted with extended chains, J. Phys. Chem. A 113 (2009) 1235–1243, http://dx.doi.org/10.1021/jp809830x.
[23] J.T. Edward, Molecular volumes and the Stokes-Einstein equation, J. Chem. Educ. 47 (1970) 261, http://dx.doi.org/10.1021/ed047p261.
[24] C. Reichardt, Solvatochromic dyes as solvent polarity indicators, Chem. Rev. 94 (1994) 2319–2358, http://dx.doi.org/10.1021/cr00032a005.
[25] B.K. Gupta, G. Kedawat, P. Kumar, M.A. Rafiee, P. Tyagi, R. Srivastava, P.M. Ajayan, An n-type, new emerging luminescent polybenzodioxane polymer for application in solution-processed green emitting OLEDs, J. Mater. Chem. C 3 (2015) 2568–2574, http://dx.doi.org/10.1039/C4TC02581D.
[26] S. Chidirala, H. Ulla, A. Valaboju, M.R. Kiran, M.E. Mohanty, M.N. Satyanarayan, G. Umesh, K. Bhanuprakash, V.J. Rao, Pyrene–oxadiazoles for organic light-emitting diodes: triplet to singlet energy transfer and role of hole-injection/hole-blocking materials, J. Org. Chem. 81 (2016) 603–614, http://dx.doi.org/10.1021/acs.joc.5b02423.
[27] J.M. Fernandes, M. Raveendra Kiran, H. Ulla, M.N. Satyanarayan, G. Umesh, Investigation of hole-injection in α-NPD using capacitance and impedance spectroscopy techniques with F4TCNQ as hole-injection layer: initial studies, Superlattices Microstruct. 76 (2014) 385–393, http://dx.doi.org/10.1016/j.spmi.2014.10.026.
[28] J.M. Fernandes, M.R. Kiran, H. Ulla, M.N. Satyanarayan, G. Umesh, Investigation of hole transport in α-NPD using impedance spectroscopy with F4TCNQ as hole-injection layer, Superlattices Microstruct. 83 (2015) 766–775, http://dx.doi.org/10.1016/j.spmi.2015.04.019.